ACS OMEGA

http://pubs.acs.org/journal/acsodf

Article

Effects of Myristate on the Induced Circular Dichroism Spectra of Aripiprazole Bound to Human Serum Albumin: A Structural–Chemical Investigation

Kenshiro Hirata,[⊥] Akito Kawai,[⊥] Victor Tuan Giam Chuang, Keiki Sakurama, Koji Nishi, Keishi Yamasaki,* and Masaki Otagiri*

Cite This: *ACS Omega* 2022, 7, 4413–4419

Read Online

ACCESS | Metrics & More | Article Recommendations | Supporting Information

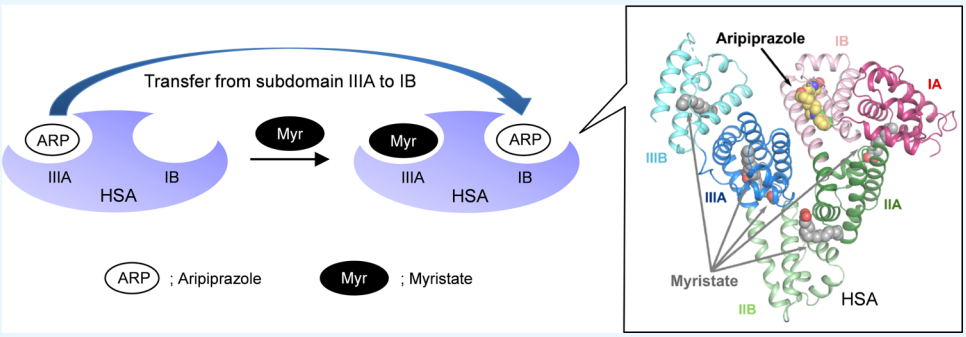

ABSTRACT: The effects of myristate on the induced circular dichroism spectra of aripiprazole (ARP) bound to human serum albumin (HSA) were investigated. High concentrations of myristate reversed the Cotton effects induced in the ARP–HSA system. The observed ellipticities increased with increasing drug concentration up to an ARP-to-HSA molar ratio of 1:1 and then decreased, indicating that the extrinsic Cotton effects were generated by the binding of ARP molecules to the high- and low-affinity sites in HSA. The data for the concentration of free ARP show that myristate displaces ARP molecules from HSA. Moreover, the free fractions of ARP in the ARP–HSA–myristate system increased significantly when adding fusidic acid, a subdomain IB ligand. In the crystal structure of the ARP–HSA–myristate ternary complex, one ARP molecule is bound to subdomain IB, and the interaction between the carbonyl group of ARP and the aromatic ring of Tyr138 in subdomain IB is essential for binding to occur. Meanwhile, the ARP molecule in the ARP–HSA binary complex structure is bound only to subdomain IIIA. Consequently, the inversion in the extrinsic Cotton effects in the ARP–HSA system can be attributed to the modification of the geometry within the binding pocket, in addition to the transfer of ARP from subdomain IIIA to subdomain IB through the displacement as a result of the binding of myristate to subdomain IIIA.

1. INTRODUCTION

Human serum albumin (HSA), the most abundant protein in the circulatory system, has one principal function, namely, to transport endogenous substances and drugs.[1] The binding of a drug to HSA is affected by some diseases and also, in some cases, by coadministered drugs. The binding affinity of drugs to HSA and the binding sites on HSA molecules are essential issues for understanding the interaction mode of drugs to HSA.[2−4] The binding of ligands to albumin is commonly examined using techniques such as equilibrium dialysis, ultrafiltration, surface plasmon resonance, spectroscopic methods, and X-ray crystallography.[5] Circular dichroism (CD) spectroscopy has been extensively used to investigate drug binding to HSA because this technique permits the protein's binding constant and conformational change upon ligand binding to be estimated.[6,7] More importantly, CD spectroscopy can shed more light on the stereochemistry of an albumin–drug complex and, thus, on the binding mechanism.

We recently reported on the binding parameters of aripiprazole (ARP), a quinolinone derivative and atypical antipsychotic drugs, to HSA.[8,9] An extrinsic positive Cotton effect for ARP bound to HSA was observed at around 265 nm, and a negative Cotton effect was observed at about 300 nm. In addition, we found that myristate caused the reversal of the induced Cotton effects of ARP–HSA. However, the mechanism underlying this change is not completely under-

Received: November 5, 2021
Accepted: January 19, 2022
Published: January 27, 2022

https://doi.org/10.1021/acsomega.1c06220
ACS Omega 2022, 7, 4413–4419

stood. Thus, we continue to study the mechanism responsible for the reversible of the Cotton effects for this ARP−HSA complex that are caused by myristate. Attempts were made to examine the interaction mode between ARP and myristate by analyzing the X-ray crystal structure of the ARP−HSA−myristate complex.

2. RESULTS

The extrinsic Cotton effects of ARP bound to HSA were again observed, as we reported in a previous report.[8] As expected, upon the addition of myristate, the induced ellipticities of the ARP−HSA system were decreased with increasing myristate concentration (10−40 μM). However, the further addition of myristate (80−120 μM) caused a change in the sign of the induced CD spectra (Figure 1).

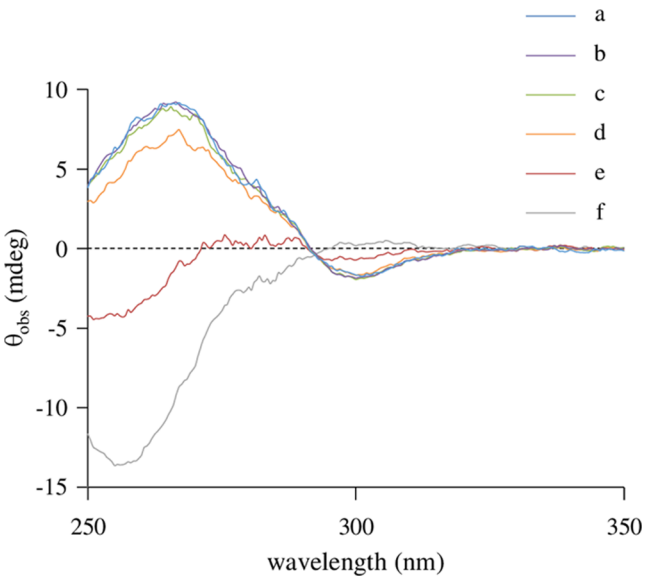

Figure 1. Effects of myristate on CD spectra for the interactions of ARP with HSA at pH 7.4 and 25 °C. The concentrations of HSA and ARP were 40 and 20 μM, respectively. The concentrations of myristate were 0 μM (a), 10 μM (b), 20 μM (c), 40 μM (d), 80 μM (e), and 120 μM (f).

In contrast, increasing the concentration of octanoate, a medium-chain fatty acid, resulted in a decrease in the observed ellipticities without showing signs of its CD spectra (Figure S1). The following experiments were then carried out to investigate the mechanism responsible for the irregular CD spectra of the ARP−HSA−myristate system. The effect of pH on the induced CD spectra of ARP−HSA was initially examined because HSA undergoes conformational changes in the physiological pH range (6.5−8.2), which are commonly referred to as the N−B transition.[10] Changes in pH, however, resulted in essentially no changes in the induced ellipticities, and a reverse of the signs of the Cotton effects was not observed (Figure S2). This observation suggests that pH-dependent conformational changes, i.e., the N−B transition, do not affect the extrinsic Cotton effects of the ARP−HSA system. The results of subsequent experiments indicated that guanidine chloride, a protein denaturant, decreased the observed ellipticities slightly and significantly but without causing any change in the signs of the Cotton effects (Figure S3). The dependency of ARP concentration was next examined because the binding of a drug to its high- versus low-affinity binding sites on HSA sometimes shows completely different Cotton effects.[11] The ARP-bound HSA induced ellipticities increased with increasing ARP concentrations (10, 20 μM), and the CD peak at around 265 nm decreased with increasing ARP concentration (40−60 μM). However, the reversal of Cotton effect signs was not observed, as shown in Figure 2. The

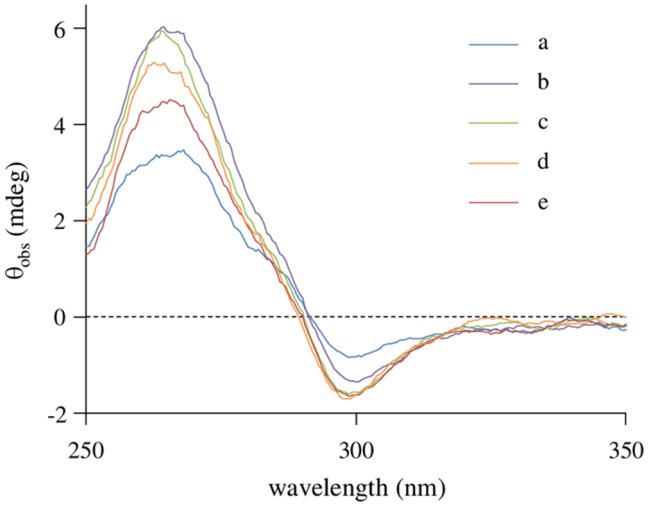

Figure 2. Effect of ARP concentration on CD spectra of the HSA−ARP system. The concentration of HSA was 20 μM, and the concentrations of ARP were 10 μM (a), 20 μM (b), 40 μM (c), 50 μM (d), and 60 μM (e).

isosbestic point at around 295 nm was observed up to an ARP-to-HSA molar ratio of 1:1, but the isosbestic point was not observed at molar ratios above 1:1. These results suggest that the change of the ellipticities shown in Figure 2 can be explained by the ellipticities involving high- and low-affinity binding sites on HSA. The ARP molecule bound to the high-affinity site in HSA generates a positive extrinsic Cotton effect at around 265 nm. The ARP molecule bound to the low-affinity site in HSA induces small ellipticities with a negative sign.

Moreover, to clarify these differences, the crystal structure of the ARP−HSA−myristate complexes was determined at a 2.30 Å resolution and refined to the final R and R_{free} factors of 21.9 and 26.1%, respectively. Data collection and structure refinement statistics are summarized in Table 1. The crystal structure of the ARP−HSA−myristate ternary complex shows that one ARP molecule is bound to subdomain IB in the HSA structure (Figure 3).

In contrast, the ARP molecule in the ARP−HSA binary complex structure is only bound to subdomain IIIA.[8] Subdomain IB of HSA is a typical drug binding site, and Carter reported that 49% of the HSA ligands that were studied by this group have at least one binding site at subdomain IB.[12] The binding site in subdomain IB has a capacity for accommodating larger heterocyclic compounds such as long-chain fatty acids, hemin, and bilirubin, compared to drug binding sites 1 and 2.[12] The area of the interface between HSA and ARP is 473.5 Å^2. The binding site for the dichlorophenyl-piperazine group of ARP is surrounded by Ile142, Arg145, His146, Phe149, Leu154, Phe157, Tyr161, Arg186, Gly189, Lys190, and Ser193 (Figure 4a). The binding site for the dihydro-quinoline group of ARP is surrounded by Arg114, Leu115, Val116, Arg117, Pro118, Met123, Phe134, Tyr138,

https://doi.org/10.1021/acsomega.1c06220
ACS Omega 2022, 7, 4413−4419

Table 1. Data Collection and Structure Refinement Statistics[d]

data set	ARP−HSA−myristate complex
data collection	
source	Photon Factory BL-17A
wavelength (Å)	0.9800
space group	*P*1
unit-cell parameters	
length (Å)	a = 38.8, b = 94.0, c = 94.9
angle (deg)	α = 105.3, β = 89.8, γ = 100.2
resolution range (Å)	50.0−2.30 (2.44−2.30)
no. of observed reflections	195 988 (29 919)
no. of unique reflections	55 157 (8844)
multiplicity	3.6 (3.4)
completeness (%)	97.3 (96.4)
R_{merge} (%)[a]	4.5 (32.9)
$\langle I/\sigma\ (I)\rangle$	14.5 (2.8)
refinement	
resolution (Å)	35.7−2.30 (2.34−2.30)
reflection used	55 117 (2632)
R_{work} (%)[b]	21.9 (30.7)
R_{free} (%)[c]	26.1 (35.4)
no. of non-hydrogen atoms	9314
protein	8853
ligands	234
solvent	227
RMSD from ideality	
bond length (Å)	0.009
bond angle (deg)	0.618
average *B*-factor	67.7
protein	67.8
ligands	72.5
solvent	60.4
Ramachandran plot	
favored region (%)	97.21
allowed region (%)	2.70
outlier region (%)	0.09
clash score	3.94

[a] $R_{merge} = 100 \times \Sigma_{hkl}\ \Sigma_i|I_i(hkl) - \langle I(hkl)\rangle|/\Sigma_{hkl}\ \Sigma_i\ I_i(hkl)$, where $\langle I(hkl)\rangle$ is the mean value of $I(hkl)$. [b] $R_{work} = 100 \times \Sigma_{hkl}||F_o| - |F_c||/\Sigma_{hkl}|F_o|$, where F_o and F_c are the observed and calculated structure factors, respectively. [c] R_{free} is calculated as for R_{work}, but the test set comprising 5% reflections was not used in the refinement. [d] Values in parentheses denote the highest-resolution shell.

Tyr161, Phe165, and Leu182 (Figure 4a). The dichlorophenyl-piperazine group and the dihydro-quinoline group of ARP are in van der Waals contact with Ile142, His146, Arg186, and Gly189 and Leu115, Arg117, Pro118, and Met123, respectively. The carbonyl group of the dihydro-quinoline group of ARP is in close proximity to the aromatic ring of Tyr138 (Figure 4b), suggesting a lone pair−π interaction.

As shown in Figure 5, we compared subdomain IB structures in the ARP−HSA−myristate complex to the HSA−fusidic acid complex structure (PDB ID 2VUF[13]). This result shows that the binding locations of these ligands are nearly identical, but the unstacking and rotating of Tyr138 and Tyr161 are only observed for the ARP−HSA−myristate complex structure. At the same time, stacking interactions between Tyr138 and Tyr161 were observed in the HSA−fusidic acid complex structure. This stacking interaction between Tyr138 and Tyr161 is also observed in the HSA structure with no ligand bound to subdomain IB. It is well known that the direct

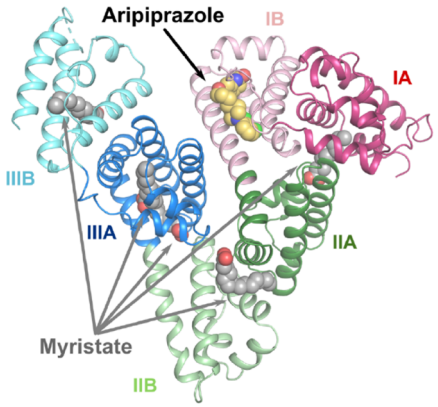

Figure 3. Overall structure of the ARP−HSA−myristate complex. The HSA structure is shown as a cartoon representation, and the subdomain structures are colored in magenta (IA), pink (IB), green (IIA), pale green (IIB), blue (IIIA), and cyan (IIIB). The ARP molecule (yellow) and the myristate molecule (gray) are shown as CPK representations.

penetration of a ligand such as a fatty acid, hemin, or delta12-prostaglandin J2 into the aromatic ring positions of Tyr138 and Tyr161 induces the disruption of the stacking interactions and causes conformational changes in these tyrosine residues.[14] In the HSA−fusidic acid complex structure, the fusidic acid molecule does not coincide with the positions of the stacking interaction between Tyr138 and Tyr161 that are observed in the HSA structure with no ligand bound to subdomain IB, and the disruption of the stacking interaction between Tyr138 and Tyr161 is not induced. The ARP molecule in the ARP−HSA−myristate complex structure does not directly penetrate into the stacking interaction position between Tyr138 and Tyr161, as is so for the HSA−fusidic acid complex. Thus, the binding of ARP to HSA does not interfere with the development of stacking interactions between Tyr138 and Tyr161. These results suggest that the binding of ARP into subdomain IB of HSA induces conformational changes in Tyr138 and Tyr161, and the interaction between the carbonyl group of ARP and the aromatic ring of Tyr138 is essential for the binding of ARP to subdomain IB of HSA.

3. DISCUSSION

When ARP was added to the HSA solution, Cotton effects appeared at around 265 and 300 nm. Since ARP is not optically active and HSA itself does not produce any Cotton effects at these wavelengths, there is no doubt that the observed Cotton effects are extrinsic in origin. Higher concentrations of myristate reversed the signs of the CD Cotton effects for this ARP−HSA system (Figure 1). Since the binding of myristate to HSA did not produce any extrinsic Cotton effects at these wavelengths, these observed CD spectral changes can be attributed to the myristate-induced allosteric modification of the ARP binding sites on the HSA molecule. Various effects on these induced ellipticities were examined to investigate the mechanism responsible for the reversal of the sign of the ARP−HSA extrinsic Cotton effects caused by myristate. The N−B transition, a pH-dependent conformational change, has little effect on the binding and/or the geometry of ARP, as evidenced by the fact that the CD spectra of the ARP−HSA system between pH 6.5 and 9.5 were nearly identical (Figure S2). Guanidine chloride decreased the observed ellipticities of the ARP−HSA system but no change

https://doi.org/10.1021/acsomega.1c06220
ACS Omega 2022, 7, 4413−4419

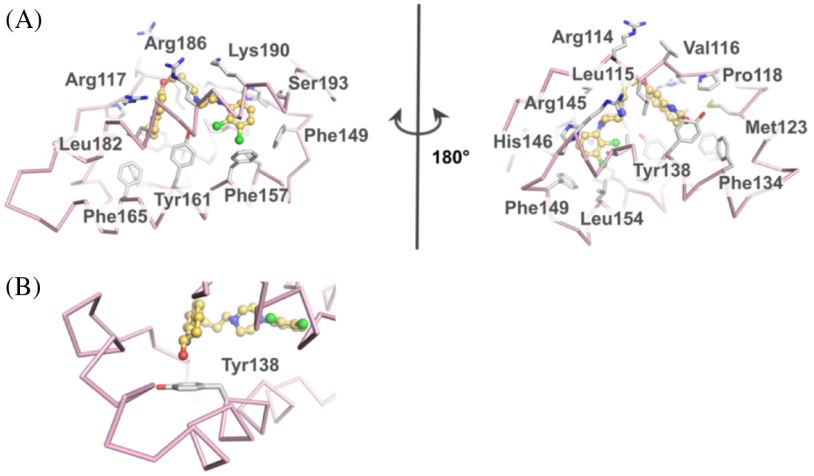

Figure 4. ARP binding at subdomain IB in HSA. (A) ARP binding at subdomain IB. The ARP molecule (yellow) is shown as a ball-and-stick representation. (B) Close-up view of the interaction between the carbonyl group of ARP and the aromatic ring of Tyr138.

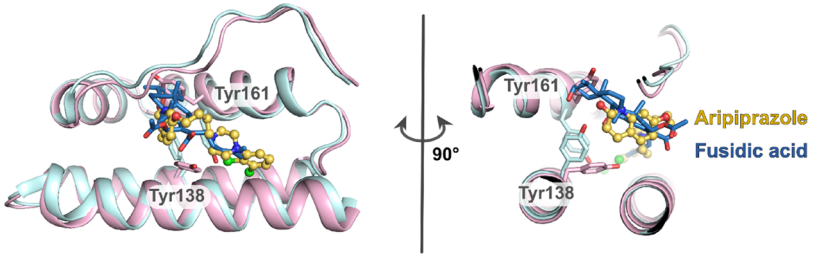

Figure 5. Structure comparison of the HSA−ARP−myristate complex with the HSA−fusidic acid complex. Protein structures of the HSA−ARP−myristate complex and the HSA−fusidic acid complex are colored in pink and cyan, respectively. The ARP molecule (yellow) is shown as a ball-and-stick representation, and the fusidic acid molecule (blue) is shown as a stick representation. The RMSD value for the corresponding 89 Ca atoms in the HSA−ARP−myristate complex structure and the HSA−fusidic acid complex structure is 0.78 Å.

in the signs of the Cotton effects was observed. The reduced intensity of the CD spectrum can be attributed to a lowering of the binding affinity rather than a change in the geometry of the binding site as a result of local conformational changes in HSA. The free fraction of ARP was increased when guanidine chloride was added to the solution (free fraction of ARP: 0.89% without guanidine chloride; 4.39% with 0.1% guanidine chloride). No changes were found in the secondary structures of HSA.

Sign changes of the drug−HSA system-induced Cotton effects can sometimes depend on the drug concentration. For example, the binding of carprofen and diclofenac to HSA caused sign changes in HSA CD spectra and these changes were dependent on the drug concentration.[11,15] For ARP, the ellipticities increased with increasing ARP concentrations, and the observed ellipticities decreased with further increases in the concentration of ARP (Figure 2). These findings clearly indicate that the ARP molecule binds to both high-affinity and low-affinity sites on HSA and generate different ellipticities. However, the reversal of the CD sign was not observed since it is difficult to increase the concentration of ARP to a level greater than 60 μM (ARP/HSA >3) because of the low solubility of the ARP molecule.

We previously reported that ibuprofen, a site II-specific drug, altered the sign of the extrinsic Cotton effects of carprofen and diclofenac bound to HSA and we proposed that this site II-to-site I displacement was the cause of the Cotton effect sign reversal.[11,15] Anti-inflammatory drugs that are displaced from their high-affinity site (site II) then become bound to lower-affinity site (site I). The binding of this drug to the high-affinity site generates positive Cotton effects, and the binding of the drug to lower-affinity sites induces negative signs. At first glance, the possibility that the above mechanism is responsible for the ARP−myristate system can be excluded because no reversal was detected in the CD spectra for ARP bound to HSA (Figure 2). However, although the reversal of the ARP−HSA system extrinsic Cotton effect sign was not found in these experimental conditions, the observed ellipticities increased up to a molar ratio (ARP/HSA) of 1:1 and then decreased for molar ratios beyond 1:1. These findings indicate that both the high-affinity site and low-affinity site are involved in the generation of the observed ellipticities. A crystallographic structural analysis of the ARP−HSA binary complex and the ARP−HSA−myristate ternary complex shows that the ARP molecule is located in the binding pocket within subdomain IIIA and subdomain IB, respectively. It is well known that subdomain IIIA functions as a low-affinity site for long-chain fatty acids such as myristate.[16,17] In addition, the ellipticity of the ARP−HSA system at 265 nm began to change markedly (positive to negative ellipticity) when the myristate-to-HSA ratio exceeded 1 (Figures 1 and S4). Taking these findings into consideration, we conclude that ARP might be displaced from subdomain IIIA (a high-affinity site for ARP) when the concentration of myristate is increased, and the resulting displaced ARP would then bind to subdomain IB (low-affinity site for ARP). Thus, it is reasonable to conclude that the reversal of the sign for the Cotton effect of the ARP−HSA

https://doi.org/10.1021/acsomega.1c06220
ACS Omega 2022, 7, 4413−4419

system caused by myristate can be explained by this site-to-site transfer mechanism.

A previous study reported that the free fraction of ARP increased markedly in the presence of octanoate, while myristate caused a slight increase in the ARP free fraction.[8] Moreover, the free fractions of ARP in the ARP−HSA−myristate system increased significantly in the presence of fusidic acid, a ligand that typically binds to subdomain IB (Figure 6). The increase in the concentration of free ARP

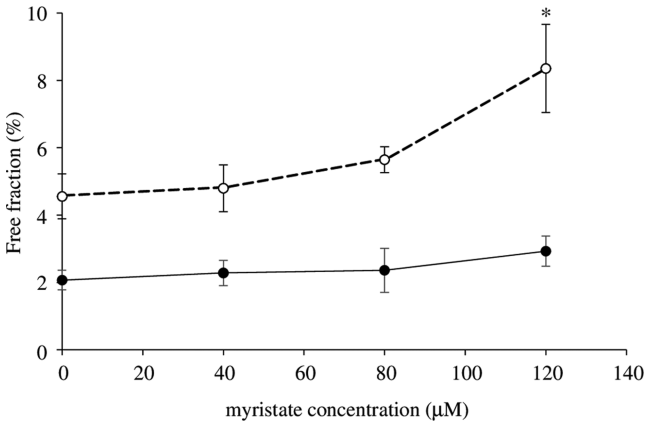

Figure 6. Effect of fusidic acid on the inhibition of ARP binding to HSA by myristate. The concentrations of HSA and ARP were 40 μM. The solid line (closed circle) represents fusidic acid (−), and the dashed line (open circle) represents 40 μM fusidic acid (+). *$p < 0.05$ as compared with fusidic acid (−) of the same concentration's myristate.

might be due to the inhibition of the rebinding to subdomain IB by fusidic acid, a subdomain IB ligand. Similar findings regarding site-to-site displacement were obtained for the ketoprofen−HSA−myristate system using a photoaffinity labeling technique at the same laboratories.[18]

Based on a crystallographic data analysis, seven binding sites for fatty acids were reported,[19,20] and the ARP molecule is bound to subdomain IIIA in the defatted HSA structure. Among these fatty acid-binding sites in HSA, octanoate binds primarily to subdomain IIIA of HSA. Five fatty acid-binding sites are known in the case of myristate, and its second high-affinity site is located at subdomain IIIA. In addition, some low-affinity binding sites were located at subdomains IA, IB, and IIB. The crystal structure of the ARP−HSA−myristate ternary complex shows that one ARP molecule is bound to subdomain IB in the HSA structure and five myristate molecules are bound to subdomains IIIB, IIIA, IIB, IIA, and IA in HSA, respectively (Figure 3).

Induced Cotton effects are often observed when the electrons of a chromophore are perturbed by electrostatic forces associated with a nearby asymmetrical locus.[21] The sign of such an induced Cotton effect, whether extrinsic or intrinsic, is governed by the configuration of the asymmetrical center and its spatial relationship to the perturbed chromophore. We recently found that deschloro-ARP, on binding to HSA, generated extrinsic Cotton effects with a negative sign. Its CD spectral characteristics are similar to that of the ARP−HSA complex in the presence of myristate.[8] ARP forms halogen bond interactions with HSA, as mentioned above. Therefore, in the case of deschloro-ARP, the geometry or configuration of this compound within the site II binding pocket is somewhat different from that of the ARP molecule after removing the chlorine atom. Thus, it is difficult to exclude the contribution of the change in the geometry of ARP within subdomain IIIA by adding myristate to the inversion in the extrinsic Cotton effects in the ARP−HSA system (Figure 1).

We previously reported on such site-to-site transfer mechanism in the case of diclofenac−ibuprofen,[11] carprofen−ibuprofen,[15] and benzbromarone−oleate.[22] The findings reported in this study provide a clearer picture of the mechanism since it is based on CD measurements in conjunction with X-ray crystallographic analysis and inhibition experiments. Taking these accumulated data into consideration, drugs for which there is no low-affinity site (e.g., diazepam) may not show the site-to-site transfer that was observed in the ARP−myristate interactions. Thus, the present study provides useful information not only for understanding the displacement mechanism but also for predicting the extent of increase in the free fraction or free concentration of a certain drug based on this mechanism.

4. CONCLUSIONS

In conclusion, the modification of the geometry within the binding pocket in addition to the mechanism responsible for the transfer from subdomain IIIA to subdomain IB through the displacement caused by the binding of myristate to subdomain IIIA (Figure 7) may be responsible for the extrinsic Cotton effect sign reversal in the case of an ARP−HSA complex.

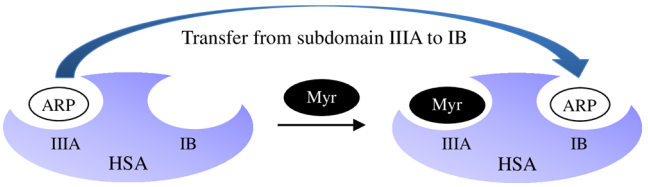

Figure 7. Schematic model of the transfer of ARP from subdomain IIIA (high-affinity site) to IB (low-affinity site) by myristate (Myr) binding to IIIA. Myristate displaces ARP from subdomain IIIA as low-affinity and high-affinity sites for myristate and ARP, respectively.

5. EXPERIMENTAL SECTION

5.1. Materials. The recombinant HSA was a gift from Nipro Co. (Shiga, Japan). Using a modification of the procedure reported by Chen,[23] HSA was defatted with activated charcoal at 4 °C in an acidic solution, deionized, and then freeze-dried. Aripiprazole (ARP) was purchased from Tokyo Chemical Industry Co. (Tokyo, Japan). Sodium myristate and sodium octanoate were purchased from Wako Pure Chemical Industries, Ltd. (Osaka, Japan). All other chemicals were purchased from commercial sources and were of the highest grade available. All solutions were prepared in deionized and distilled waters.

5.2. Circular Dichroism Measurement. CD measurements were made on a Jasco model J-720 spectropolarimeter (Tokyo, Japan) using 10 mm cell at 25 °C. Observed ellipticity was defined as the ellipticity (in degrees) of an ARP−HSA mixture (10−60 μM ARP, 20 μM HSA) minus the ellipticity of HSA alone within the same wavelength region. We used ARP concentrations of less than 60 μM because of the limited solubility of ARP. The measurements were performed with a data interval of 0.1 nm, a scanning speed of 50 nm/min, a response time of 4 s, and a bandwidth of 1.0 nm.

https://doi.org/10.1021/acsomega.1c06220
ACS Omega 2022, 7, 4413−4419

5.3. Equilibrium Dialysis. Equilibrium dialysis experiments were conducted following a previously described method.[8] Briefly, aliquots (0.5 mL) of samples (40 μM HSA, 40 μM ARP, 0−120 μM myristate), in 2 mL Sanko plastic cells (Fukuoka, Japan), were dialyzed at 25 °C for 12 h against the same volume of buffer solution. After reaching equilibrium, the drug concentration in the buffer (D_f; unbound ARP concentration) and HSA compartments (D_{b+f}; the sum of the bound and unbound ARP concentrations) was determined by HPLC. The free fraction (%) was calculated using the following equation

$$\text{free fraction (\%)} = D_f/D_{b+f} \times 100 \quad (1)$$

5.4. Crystallization of the ARP−HSA−Myristate Complex. Preparation of the HSA solution for the crystallization was performed as described in a previous report.[24,25] ARP solution (50 mM) was prepared by dissolving it in DMSO. A nominal concentration of 2 mM of the myristate suspension in 50 mM potassium phosphate buffer (pH 7.0) was prepared by heating to 60 °C and vortexing, followed by cooling to around 37 °C. The ARP−HSA−myristate complex was formed by mixing the HSA solution, 50 mM of the ARP solution, and the myristate suspension at a 1:13:13 ARP/HSA/myristate molar ratio in 50 mM potassium phosphate buffer pH 7.0 and 10% (v/v) DMSO, and the resulting solution was then incubated at 20 °C overnight. After incubation, excess unbound and insoluble ARP and myristate depositions were removed by centrifugation (18 800g for 1 h at 4 °C), and the ARP−HSA−myristate complex was washed with 50 mM potassium phosphate buffer at pH 7.0 by performing two cycles of dilution and concentration using a Vivaspin 500 (MWCO 10 000, Sartorius) centrifugal concentrator. The solution of the ARP−HSA−myristate complex was finally concentrated to 1.4 mM of the HSA concentration. Cocrystallization of the ARP−HSA−myristate complex was performed using the hanging-drop vapor diffusion method, and ARP−HSA−myristate crystals suitable for X-ray analysis were obtained by multiple rounds of streak-seeding with droplets prepared by mixing 1.5 μL of the ARP−HSA−myristate solution and 1.5 μL of the reservoir solution containing 32% (w/v) poly(ethylene glycol) 3350 and 50 mM potassium phosphate buffer pH 7.0 at 4 °C and pre-equilibrated for 1 day.

5.5. Data Collection, Structure Determination, and Refinement. The ARP−HSA−myristate crystals were directly frozen in liquid nitrogen. Synchrotron experiments were performed at Photon Factory BL-17A (Tsukuba, Japan). Diffraction data sets were collected at −173 °C using an Eiger X 16M detector, and the data sets were processed and scaled using *XDS*.[26] The initial phase of the ARP−HSA−myristate complex structure was determined by the molecular replacement method using *MOLREP*[27] from the *CCP*4 program suite,[28] with the coordinate (PDB: 1BJ5[29]) serving as the search model. Another model building was performed with *COOT*.[30] Structure refinement, including the refinement of atomic displacement parameters by the translation, liberation, and screw (TLS) method, was performed with *phenix.refine*.[31] TLS groups were determined using *phenix.find_tls_groups* from the *PHENIX* package.[32] The stereochemical quality of the final structure was evaluated by *MolProbity*[33] All molecular graphics were prepared using *PyMOL*.[34] Structure analysis including the calculation of the interface area between HSA and ARP was performed with PDBePISA.[35] The atomic coordinates of the ARP−HSA−myristate complex were deposited in the Protein Data Bank under the accession code 7VR9.

5.6. Statistical Analysis. Statistical analyses were performed with EZR (Saitama Medical Center, Jichi Medical University, Saitama, Japan).[36] Regarding the effect of fusidic acid on the inhibition of the binding of ARP to HSA by myristate, to evaluate the presence or absence of fusidic acid, we performed the Mann−Whitney test at each concentration of myristate.

■ ASSOCIATED CONTENT

Supporting Information

The Supporting Information is available free of charge at https://pubs.acs.org/doi/10.1021/acsomega.1c06220.

Effects of octanoate, pH change, and guanidine chloride on CD spectra for the interactions of ARP with HSA; and the effect of myristate on the ellipticity at 265 nm for the interactions of ARP with HAS (PDF)

■ AUTHOR INFORMATION

Corresponding Authors

Keishi Yamasaki − *Faculty of Pharmaceutical Sciences, Sojo University, Kumamoto 860-0082, Japan; DDS Research Institute, Sojo University, Kumamoto 860-0082, Japan;* orcid.org/0000-0003-0537-2367; Email: kcyama@ph.sojo-u.ac.jp

Masaki Otagiri − *Faculty of Pharmaceutical Sciences, Sojo University, Kumamoto 860-0082, Japan; DDS Research Institute, Sojo University, Kumamoto 860-0082, Japan;* Email: otagirim@ph.sojo-u.ac.jp

Authors

Kenshiro Hirata − *Faculty of Pharmaceutical Sciences, Sojo University, Kumamoto 860-0082, Japan;* orcid.org/0000-0002-8963-2228

Akito Kawai − *Fujita Health University School of Medicine, Toyoake, Aichi 470-1192, Japan*

Victor Tuan Giam Chuang − *Discipline of Pharmacy, Curtin Medical School, Faculty of Health Sciences, Curtin University, Perth, Western Australia 6845, Australia*

Keiki Sakurama − *Faculty of Pharmaceutical Sciences, Sojo University, Kumamoto 860-0082, Japan*

Koji Nishi − *Faculty of Pharmaceutical Sciences, Sojo University, Kumamoto 860-0082, Japan*

Complete contact information is available at: https://pubs.acs.org/10.1021/acsomega.1c06220

Author Contributions

⊥K.H. and A.K. contributed equally.

Notes

The authors declare no competing financial interest.

■ ACKNOWLEDGMENTS

Synchrotron experiments were performed with the approval of the Photon Factory Program Advisory Committee (Proposal Nos. 2017G554 and 2019G592). The authors are grateful to the beamline staff for their support of our synchrotron experiments.

REFERENCES

(1) Kragh-Hansen, U.; Chuang, V. T. G.; Otagiri, M. Practical Aspects of the Ligand-Binding and Enzymatic Properties of Human Serum Albumin. *Biol. Pharm. Bull.* **2002**, *25*, 695−704.

(2) Jusko, W. J.; Gretch, M. Plasma and Tissue Protein Binding of Drugs in Pharmacokinetics. *Drug Metab. Rev.* **1976**, *5*, 43−140.

(3) Otagiri, M. A Molecular Functional Study on the Interactions of Drugs with Plasma Proteins. *Drug Metab. Pharmacokinet.* **2005**, *20*, 309−323.

(4) Yamasaki, K.; Chuang, V. T. G.; Maruyama, T.; Otagiri, M. Albumin-Drug Interaction and Its Clinical Implication. *Biochim. Biophys. Acta* **2013**, *1830*, 5435−5443.

(5) Chuang, V. T. G.; Maruyama, T.; Otagiri, M. Updates on Contemporary Protein Binding Techniques. *Drug Metab. Pharmacokinet.* **2009**, *24*, 358−364.

(6) Yao, H.; Wynendaele, E.; Xu, X.; Kosgei, A.; De Spiegeleer, B. Circular Dichroism in Functional Quality Evaluation of Medicines. *J. Pharm. Biomed. Anal.* **2018**, *147*, 50−64.

(7) Zsila, F. Circular Dichroism Spectroscopic Detection of Ligand Binding Induced Subdomain IB Specific Structural Adjustment of Human Serum Albumin. *J. Phys. Chem. B* **2013**, *117*, 10798−10806.

(8) Sakurama, K.; Kawai, A.; Tuan Giam Chuang, V.; Kanamori, Y.; Osa, M.; Taguchi, K.; Seo, H.; Maruyama, T.; Imoto, S.; Yamasaki, K.; Otagiri, M. Analysis of the Binding of Aripiprazole to Human Serum Albumin: The Importance of a Chloro-Group in the Chemical Structure. *ACS Omega* **2018**, *3*, 13790−13797.

(9) Sakurama, K.; Nishi, K.; Imoto, S.; Hashimoto, M.; Komatsu, T.; Morita, Y.; Taguchi, K.; Otagiri, M.; Yamasaki, K. Further Evidence Regarding the Important Role of Chlorine Atoms of Aripiprazole on Binding to the Site II Area of Human Albumin. *J. Pharm. Sci.* **2019**, *108*, 1890−1895.

(10) Bos, O. J. M.; Labro, J. F. A.; Fischer, M. J. E.; Wilting, J.; Janssen, L. H. M. The Molecular Mechanism of the Neutral-to-Base Transition of Human Serum Albumin: Acid/Base Titration and Proton Nuclear Magnetic Resonance Studies on a Large Peptic and a Large Tryptic Fragment of Albumin. *J. Biol. Chem.* **1989**, *264*, 953−959.

(11) Yamasaki, K.; Rahman, M. H.; Tsutsumi, Y.; Maruyama, T.; Ahmed, S.; Kragh-Hansen, U.; Otagiri, M. Circular Dichroism Simulation Shows a Site-II-to-Site-I Displacement of Human Serum Albumin-Bound Diclofenac by Ibuprofen. *AAPS PharmSciTech* **2000**, *1*, No. E12.

(12) Carter, D. C. Crystallographic Survey of Albumin Drug Interaction and Preliminary Applications in Cancer Chemotherapy. In *Burger's Medicinal Chemistry and Drug Discovery*; Wiley, 2010; pp 437−468.

(13) Zunszain, P. A.; Ghuman, J.; McDonagh, A. F.; Curry, S. Crystallographic Analysis of Human Serum Albumin Complexed with 4Z,15E-Bilirubin-IXalpha. *J. Mol. Biol.* **2008**, *381*, 394−406.

(14) Yamaguchi, S.; Aldini, G.; Ito, S.; Morishita, N.; Shibata, T.; Vistoli, G.; Carini, M.; Uchida, K. Delta12-Prostaglandin J2 as a Product and Ligand of Human Serum Albumin: Formation of an Unusual Covalent Adduct at His146. *J. Am. Chem. Soc.* **2010**, *132*, 824−832.

(15) Rahman, M. H.; Maruyama, T.; Okada, T.; Yamasaki, K.; Otagiri, M. Study of Interaction of Carprofen and Its Enantiomers with Human Serum Albumin–I. Mechanism of Binding Studied by Dialysis and Spectroscopic Methods. *Biochem. Pharmacol.* **1993**, *46*, 1721−1731.

(16) Krenzel, E. S.; Chen, Z.; Hamilton, J. A. Correspondence of Fatty Acid and Drug Binding Sites on Human Serum Albumin: A Two-Dimensional Nuclear Magnetic Resonance Study. *Biochemistry* **2013**, *52*, 1559−1567.

(17) Yamasaki, K.; Hyodo, S.; Taguchi, K.; Nishi, K.; Yamaotsu, N.; Hirono, S.; Chuang, V. T. G.; Seo, H.; Maruyama, T.; Otagiri, M. Long Chain Fatty Acids Alter the Interactive Binding of Ligands to the Two Principal Drug Binding Sites of Human Serum Albumin. *PLoS One* **2017**, *12*, No. e0180404.

(18) Chuang, V. T. G.; Otagiri, M. How Do Fatty Acids Cause Allosteric Binding of Drugs to Human Serum Albumin? *Pharm. Res.* **2002**, *19*, 1458−1464.

(19) Bhattacharya, A. A.; Grüne, T.; Curry, S. Crystallographic Analysis Reveals Common Modes of Binding of Medium and Long-Chain Fatty Acids to Human Serum Albumin. *J. Mol. Biol.* **2000**, *303*, 721−732.

(20) Petitpas, I.; Grüne, T.; Bhattacharya, A. A.; Curry, S. Crystal Structures of Human Serum Albumin Complexed with Monounsaturated and Polyunsaturated Fatty Acids. *J. Mol. Biol.* **2001**, *314*, 955−960.

(21) Chignell, C. F. Optical Studies of Drug-Protein Complexes. *Mol. Pharmacol.* **1970**, *6*, 455−462.

(22) Yamasaki, K.; Kawai, A.; Sakurama, K.; Udo, N.; Yoshino, Y.; Saito, Y.; Tsukigawa, K.; Nishi, K.; Otagiri, M. Interaction of Benzbromarone with Subdomains IIIA and IB/IIA on Human Serum Albumin as the Primary and Secondary Binding Regions. *Mol. Pharmaceutics* **2021**, *18*, 1061−1070.

(23) Chen, R. F. Removal of Fatty Acids from Serum Albumin by Charcoal Treatment. *J. Biol. Chem.* **1967**, *242*, 173−181.

(24) Kawai, A.; Chuang, V. T. G.; Kouno, Y.; Yamasaki, K.; Miyamoto, S.; Anraku, M.; Otagiri, M. Crystallographic Analysis of the Ternary Complex of Octanoate and N-Acetyl-l-Methionine with Human Serum Albumin Reveals the Mode of Their Stabilizing Interactions. *Biochim. Biophys. Acta* **2017**, *1865*, 979−984.

(25) Curry, S. Lessons from the Crystallographic Analysis of Small Molecule Binding to Human Serum Albumin. *Drug Metab. Pharmacokinet.* **2009**, *24*, 342−357.

(26) Kabsch, W. XDS. *Acta Crystallogr., Sect. D: Biol. Crystallogr.* **2010**, *66*, 125−132.

(27) Vagin, A.; Teplyakov, A. *MOLREP*: An Automated Program for Molecular Replacement. *J. Appl. Crystallogr.* **1997**, *30*, 1022−1025.

(28) Winn, M. D.; Ballard, C. C.; Cowtan, K. D.; Dodson, E. J.; Emsley, P.; Evans, P. R.; Keegan, R. M.; Krissinel, E. B.; Leslie, A. G. W.; McCoy, A.; McNicholas, S. J.; Murshudov, G. N.; Pannu, N. S.; Potterton, E. A.; Powell, H. R.; Read, R. J.; Vagin, A.; Wilson, K. S. Overview of the CCP4 Suite and Current Developments. *Acta Crystallogr., Sect D: Biol. Crystallogr.* **2011**, *67*, 235−242.

(29) Curry, S.; Mandelkow, H.; Brick, P.; Franks, N. Crystal Structure of Human Serum Albumin Complexed with Fatty Acid Reveals an Asymmetric Distribution of Binding Sites. *Nat. Struct. Biol.* **1998**, *5*, 827−835.

(30) Emsley, P.; Lohkamp, B.; Scott, W. G.; Cowtan, K. Features and Development of Coot. *Acta Crystallogr., Sect D: Biol. Crystallogr.* **2010**, *66*, 486−501.

(31) Afonine, P. V.; Grosse-Kunstleve, R. W.; Echols, N.; Headd, J. J.; Moriarty, N. W.; Mustyakimov, M.; Terwilliger, T. C.; Urzhumtsev, A.; Zwart, P. H.; Adams, P. D. Towards Automated Crystallographic Structure Refinement with Phenix.Refine. *Acta Crystallogr., Sect D: Biol. Crystallogr.* **2012**, *68*, 352−367.

(32) Adams, P. D.; Afonine, P. V.; Bunkóczi, G.; Chen, V. B.; Davis, I. W.; Echols, N.; Headd, J. J.; Hung, L.-W.; Kapral, G. J.; Grosse-Kunstleve, R. W.; McCoy, A. J.; Moriarty, N. W.; Oeffner, R.; Read, R. J.; Richardson, D. C.; Richardson, J. S.; Terwilliger, T. C.; Zwart, P. H. PHENIX: A Comprehensive Python-Based System for Macromolecular Structure Solution. *Acta Crystallogr., Sect D: Biol. Crystallogr.* **2010**, *66*, 213−221.

(33) Davis, I. W.; Leaver-Fay, A.; Chen, V. B.; Block, J. N.; Kapral, G. J.; Wang, X.; Murray, L. W.; Arendall, W. B.; Snoeyink, J.; Richardson, J. S.; Richardson, D. C. MolProbity: All-Atom Contacts and Structure Validation for Proteins and Nucleic Acids. *Nucleic Acids Res.* **2007**, *35*, W375−W383.

(34) DeLano, W. L. *The PyMOL Molecular Graphics Viewing System*, Version 2.0.4; Schrödinger LLC, 2017.

(35) Krissinel, E.; Henrick, K. Inference of Macromolecular Assemblies from Crystalline State. *J. Mol. Biol.* **2007**, *372*, 774−797.

(36) Kanda, Y. Investigation of the Freely Available Easy-to-Use Software "EZR" for Medical Statistics. *Bone Marrow Transplant.* **2013**, *48*, 452−458.

https://doi.org/10.1021/acsomega.1c06220
ACS Omega 2022, 7, 4413−4419